ACS APPLIED MATERIALS & INTERFACES
Research Article
Cite This: ACS Appl. Mater. Interfaces 2017, 9, 38977-38983
www.acsami.org

Schottky Barrier Height of Pd/MoS_2 Contact by Large Area Photoemission Spectroscopy

Hong Dong,[†] Cheng Gong,[‡] Rafik Addou,[‡] Stephen McDonnell,[‡] Angelica Azcatl,[‡] Xiaoye Qin,[‡] Weichao Wang,[†] Weihua Wang,[†] Christopher L. Hinkle,[‡] and Robert M. Wallace*,[‡]

[†]Department of Electronics and Tianjin Key Laboratory of Photo-Electronic Thin Film Device and Technology, Nankai University, Tianjin 300071, China

[‡]Department of Materials Science and Engineering, University of Texas at Dallas, Richardson, Texas 75080, United States

Supporting Information

ABSTRACT: MoS_2, as a model transition metal dichalcogenide, is viewed as a potential channel material in future nanoelectronic and optoelectronic devices. Minimizing the contact resistance of the metal/MoS_2 junction is critical to realizing the potential of MoS_2-based devices. In this work, the Schottky barrier height (SBH) and the band structure of high work function Pd metal on MoS_2 have been studied by *in situ* X-ray photoelectron spectroscopy (XPS). The analytical spot diameter of the XPS spectrometer is about 400 μm, and the XPS signal is proportional to the detection area, so the influence of defect-mediated parallel conduction paths on the SBH does not affect the measurement. The charge redistribution by Pd on MoS_2 is detected by XPS characterization, which gives insight into metal contact physics to MoS_2 and suggests that interface engineering is necessary to lower the contact resistance for the future generation electronic applications.

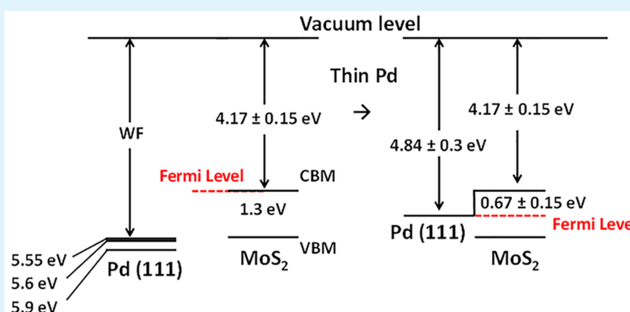

KEYWORDS: *SBH, Pd contact, MoS_2, XPS, thin film*

INTRODUCTION

Transition metal dichalcogenides (TMDs) are a family of promising 2D materials for future low power logic electronic device applications due to their predicted low concentration of surface dangling bonds, tunable band gaps, and band alignments through the proper choice of metal and chalcogen as well as their intrinsic scalability to stable, monolayer thickness.[1−5] MoS_2 is one of the most studied TMDs due to its natural abundance.[6−9] The reported metal−MoS_2 contact resistance is 10 times higher than that of Si contacts.[10,11] Thus, the high contact resistance is a hurdle to achieving the low power application potential of these materials.

Research on a reliable p-doping method without damage to the MoS_2 materials is still underway.[12,13] A proper metal contact is expected to lower the contact resistance by reducing the Schottky barrier height (SBH) and thus increase the charge carrier injection rates. The small lattice mismatch of Pd to MoS_2[14] and its high work function motivated the electrical measurement using Pd as the p-type metal contact on MoS_2, and SBH behavior is reported in the literature.[15]

Tung et al.[15,16] pointed out years ago that the SBH usually cannot be predicted by simple work function arguments on traditional semiconductors such as Si, Ge, and III−V. Similarly, DFT simulations by Kang et al.[10] and Gong et al.[17] pointed out that the simple Schottky−Mott theory cannot predict the behavior of a Pd contacts to an ideal single layer MoS_2 surface because of the charge redistribution at the metal−MoS_2 interface and the resultant overlap of the wave functions for the two contacting materials.[18,19] Their calculations indicate that the effective Pd metal work function near the middle of the monolayer MoS_2 band gap.

Many electrical measurements have been carried out to study metal−MoS_2 contact resistance.[1,6,13,20,21] High performance n-type metal contacts have been reported, but p-type contacts with high performance are not regularly reported.[12,13,20,22,23] Fontana et al. reported p-type behavior of Pd on MoS_2, consistent with simple metal work function arguments. However, other groups reported a n-type behavior for Pd, with a range of different SBH values.[20,24]

McDonnell et al. highlighted that electrical measurements are extremely sensitive to the natural doping variations in the MoS_2 itself. It was found that on a single piece of MoS_2 with simultaneously deposited Au contacts separated by only 1.25 mm that one contact exhibited n-type $I-V$ characteristics while the other exhibited p-type $I-V$ characteristics.[25] These doping variations were correlated with observable variations in defect

Received: July 27, 2017
Accepted: October 16, 2017
Published: October 16, 2017

Downloaded via UNIV OF MARYLAND COLG PARK on June 7, 2020 at 22:52:18 (UTC).
See https://pubs.acs.org/sharingguidelines for options on how to legitimately share published articles.

ACS Publications © 2017 American Chemical Society

density and stoichiometry. They proposed an alternative explanation for the apparent work function change of metals to below the conduction band of n-type MoS_2[26] by considering parallel conduction paths involving surface defects that can explain the low Schottky barrier height observed even when using high vacuum work function metals. Later work highlighted that the large level of natural impurities in the geological MoS_2 likely plays a major role in the local Fermi-level variations in MoS_2.[27]

To minimize the impact of bulk defects in the MoS_2[27] when extracting the SBH from electrical measurements, we perform an alternative measurement[28] of the SBH of Pd on bulk MoS_2 utilizing monochromatic X-ray photoelectron spectroscopy (XPS).[29,30] The surface sensitivity of XPS enables a direct measurement of the SBH, as the majority of the detected photoelectrons originate from the top surface (∼5 nm) for the analysis parameters employed here. This information depth is also coincident with the few layer devices reported in the literature. This measurement of the SBH provides new understanding of this metal−semiconductor contact.

Two *in situ* ultrahigh vacuum (UHV) surface analysis systems are used in this study to avoid spurious contamination of the MoS_2 surface. In the first UHV system ("UHV I"), a water-cooled, metal electron-beam (e-beam) evaporation source is utilized in the physical vapor deposition chamber (PVD chamber) for Pd deposition (99.95%, from Kurt J. Lesker[31]) and XPS system are connected by a UHV tube (10^{-11} mbar). A monochromatic Al Kα_1 X-ray source ($h\nu$ = 1486.7 eV) with a Omicron 125 mm hemispherical analyzer is employed for XPS, and the details of this UHV deposition/analysis cluster tool are described elsewhere.[32] The PVD chamber is equipped with reflection high-energy electron diffraction (RHEED) instrumentation to study the surface structure. The takeoff angle for XPS is 45°, and the pass energy is 15 eV under the constant analysis energy (CAE) mode. The base pressure is 10^{-10} mbar, and the pressure during e-beam evaporation is <3 × 10^{-8} mbar. The MoS_2 flake (purchased from SPI[33]) was about 1 cm^2 and 4 mm thick. After the sample was mounted on a metal plate, Scotch tape was used to peal the surface layers off to exfoliate (the sample still is ∼4 mm thick). The sample was transferred to the load lock within 5 min.

XPS was carried out on the sample after 5 and 75 min of e-beam evaporation of Pd. The RHEED study of the surface was performed after 5, 15, 25, 35, 45, 55, 65, and 75 min of Pd deposition at room temperature. The e-beam power, which is correlated to the Pd flux, was kept constant (243 W), so the thickness of the Pd deposition was controlled by the Pd flux exposure time.

Measurements were also carried out in a second, independent surface analysis UHV system ("UHV II") capable of atomic resolution studies, also described in detail elsewhere.[34,35] The apparatus has scanning tunneling microscopy (STM) as well as monochromatic XPS and an integrated preparation chamber with an e-beam evaporation source (manufactured by Oxford) also with Pd. The same XPS data acquisition parameters were also employed on both XPS instruments for this study. The exfoliated MoS_2 sample used in this case was provided by Nano Science Instruments.[36] The STM and XPS analyses were performed after 6 s, 12 s, 72 s, 180 s, 600 s, 1 h, and 3 h of Pd deposition. The XPS data analysis was carried out utilizing the peak fitting software AAnalyzer,[37] and both monochromatic XPS spectrometers were calibrated routinely with the same ASTM standard procedure.[38] The STM images and the corresponding XPS measurements[39] thus provide the detailed evolution of band bending upon the deposition.

RESULTS AND DISCUSSION

Figure 1 shows a simple Schottky barrier model schematic band structure for an n-type semiconductor with a metal contact,[15]

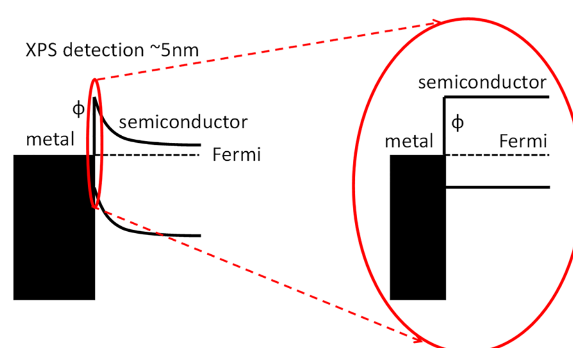

Figure 1. Simplified example model of traditional Schottky barrier diagram, where the XPS detection thickness is less than ∼5 nm due to the photoelectron inelastic mean free path. ϕ represents the Schottky barrier height of metal contact with a semiconductor. As a result, the barrier can be essentially detected by XPS.

where the depletion depth in the semiconductor is in the micrometer range. Because XPS can only detect photoelectrons from a shallow surface depth as mentioned above, band bending over this near surface region is effectively negligible, enabling accurate SBH measurements. After proper calibration of the XPS spectrometer, the position of the valence band maximum with respect to the E_F (0 eV in the XPS spectra) can be directly measured before the metal deposition.

The shift in the core-level spectra of the semiconductor after the metal deposition can then be used to monitor the near-surface Fermi-level shift caused by the formation of the Schottky junction. If the band gap of the semiconductor is known, the SBH can be then be determined directly from this measurement. It is worth noting that this method of measuring the SBH sums linearly with the local SBH area over the entire analytical spot size, in contrast to electrical measurements which are exponentially dependent on the SBH, giving much greater weight to low SBH (such as from defects) even when in low concentration.[22] Assuming the initial semiconductor is n-type, the electron SBH is defined as the metal work function minus the electron affinity of semiconductor. As seen in Figure 1, since the Fermi level of metal and the semiconductor are aligned in equilibrium, the SBH can be determined from the conduction band minimum (CBM) minus the measured surface Fermi level position, $E_{CBM} - E_F$.

Figure 2 shows the Mo 3d and S 2s core level features observed at seven random locations across an ∼10 × 10 mm area of bulk MoS_2. As previously reported, features corresponding to both p- and n-type regions are observed (Figure 2a). After a 5 min Pd deposition, estimated by the attenuation of the Mo 3d spectra to be ∼1 ML thick, the binding energy variations in the Mo 3d spectral envelope at the seven locations are observed to all "line up" at the same binding energy (229.30 eV). Band bending at the surface results in the core levels aligning as expected when forming a Schottky junction. Also, the core level peaks also show no chemical bonding of Pd to the MoS_2, consistent with previous reports.[25]

DOI: 10.1021/acsami.7b10974
ACS Appl. Mater. Interfaces 2017, 9, 38977−38983

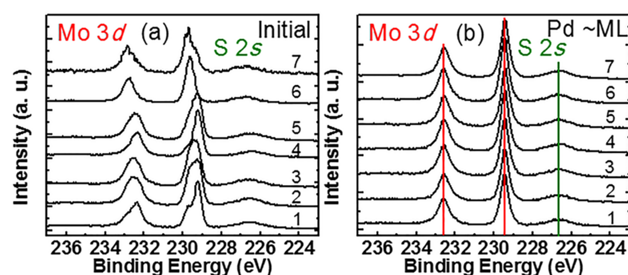

Figure 2. Mo 3d spectra for initial (a) MoS_2 at seven random XPS detection locations and (b) after a thin (∼1 ML) layer of Pd deposition on the same sample with random XPS detection locations.

Figure 3a shows the valence band structure of MoS_2 for the initial surface and then after 6, 12, and 72 s of Pd deposition.

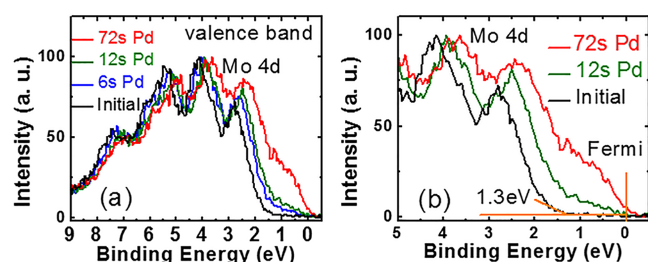

Figure 3. Valence band structure of MoS_2 for (a) the initial surface after 6, 12, and 72 s of Pd deposition and (b) valence band edge structure from (a).

The Mo 4d spectral evolution is seen and attributed to the metallic feature from the Pd deposition. The clear demonstration of VBM cutoff is shown in Figure 3b. A 1.3 eV separation from the Fermi level to VBM of MoS_2 before the metal deposition is measured in this study, indicating a Fermi level near the CBM of the MoS_2 (i.e., heavily n-type "doped"). We also measured the Mo 3d spectrum prior to Pd deposition, with a peak observed at 229.97 ± 0.05 eV, which is shown in Figure 4 as the "initial" spectrum.

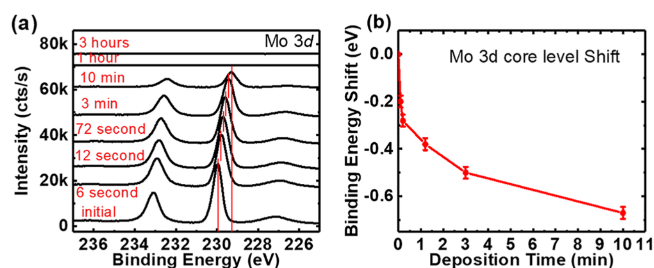

Figure 4. (a) Core level spectra of Mo 3d for the initial surface after 6 s, 12 s, 72 s, 3 min, 10 min, 1 h, and 3 h of Pd deposition and (b) core level shift with deposition time.

A shift to lower binding energies is observed with Pd deposition, as shown in Figure 4a. The core level binding energy shift is consistent with that of the valence band spectra as shown in Figure 3. Figure 4b shows the binding energy shift as a function of deposition time. The minimum binding energy position after 10 min of Pd deposition is 229.30 eV, so the final binding energy shift relative to the initial surface is 229.97 − 229.30 = 0.67 eV. This final binding energy value is also consistent with that measured in UHV I. The final Mo $3d_{5/2}$ spectra after thick Pd deposition also lines up at 229.3 eV as seen in the Supporting Information (Figure S1). The spectra of Mo 3d is attenuated below the detection limit of the XPS after the 1 and 3 h of Pd deposition shown in Figure 4.

An important property in this analysis is a consideration of the vacuum work function. The work function of Pd is strongly dependent on the crystal orientation. For example, Hulse et al.[40] reported 5.2 eV for Pd (110), 5.65 eV for Pd (100), and 5.9 eV for Pd (111); Demuth et al.[41] reported 5.6 eV for Pd (111); and Kubiak[42] reported 5.55 eV for Pd (111). Nieuwenhuys et al.[43] measured the work function of Pd film to be 5.12 eV, by evaporation of Pd onto a glass substrate (not likely resulting in a Pd(111) orientation), followed by adsorption of Xe gas at low temperature, and annealing to 297 K. Nieuwenhuys et al.'s result for the work function of Pd is reviewed by Michaelson[44] and is subsequently used in many recent publications. However, in this work, as will be shown later from RHEED patterns, the Pd film on MoS_2 has a (111) orientation. This epitaxial growth of Pd (111) on MoS_2 (0001) is also consistent with the *in situ* STM and TEM work by Perrot et al.[39] Figure 5 shows the band diagram of Pd and MoS_2 before and after contacting the metal and the semiconductor. The reported work functions of Pd (111) from the references are also listed.

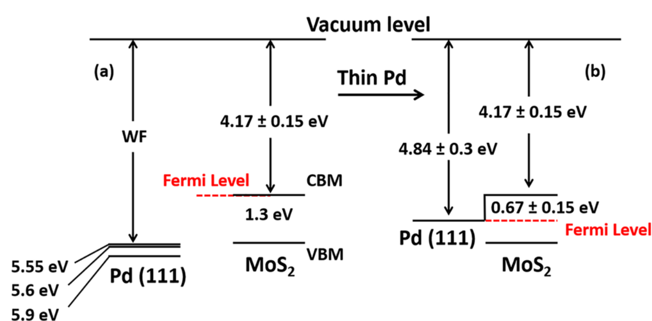

Figure 5. Band diagram of the Pd separated from MoS_2 (a) and after Pd deposition (b) as measured by XPS from UHV II. The work function values for Pd listed as 5.55, 5.6, and 5.9 eV are from the literature,[40−42] and the electron affinity is inferred from the photoionization energy given by Schlaf et al.[45]

Considering bulk MoS_2, the photoionization energy is reported[45,46] to be 5.47 ± 0.15 eV. As the band gap of bulk MoS_2 is assumed to be 1.3 ± 0.1 eV,[47,48] the electron affinity of bulk MoS_2 can be inferred to be 4.17 ± 0.15 eV. We assume the electron affinity remains constant before and during the Pd deposition process. Considering the XPS resolution for the peak position measurement, which is 0.05 eV, and the error bar of the band gap (±0.1 eV) used, the SBH is thus measured to be 0.67 ± 0.15 eV from the CBM, which is close to the middle of the band gap of MoS_2. The detailed band structure deduced from this method is shown in Figure 5a before and Figure 5b after Pd deposition from the measurement in UHV II. The effective work function of Pd is thus seen to be 4.84 ± 0.3 eV rather than in the range 5.55−5.9 eV, which would be expected for Pd (111) from the literature reports.

The predicted SBH of Pd on MoS_2, based on the simple vacuum work function argument, is thus shown to be incorrect when compared to experiment. The measured SBH is consistent with those predicted by Kang[10] and Gong[17] et al. using DFT calculations on single-layer MoS_2, which results from charge redistribution at the Pd/MoS_2 interface.

DOI: 10.1021/acsami.7b10974
ACS Appl. Mater. Interfaces 2017, 9, 38977−38983

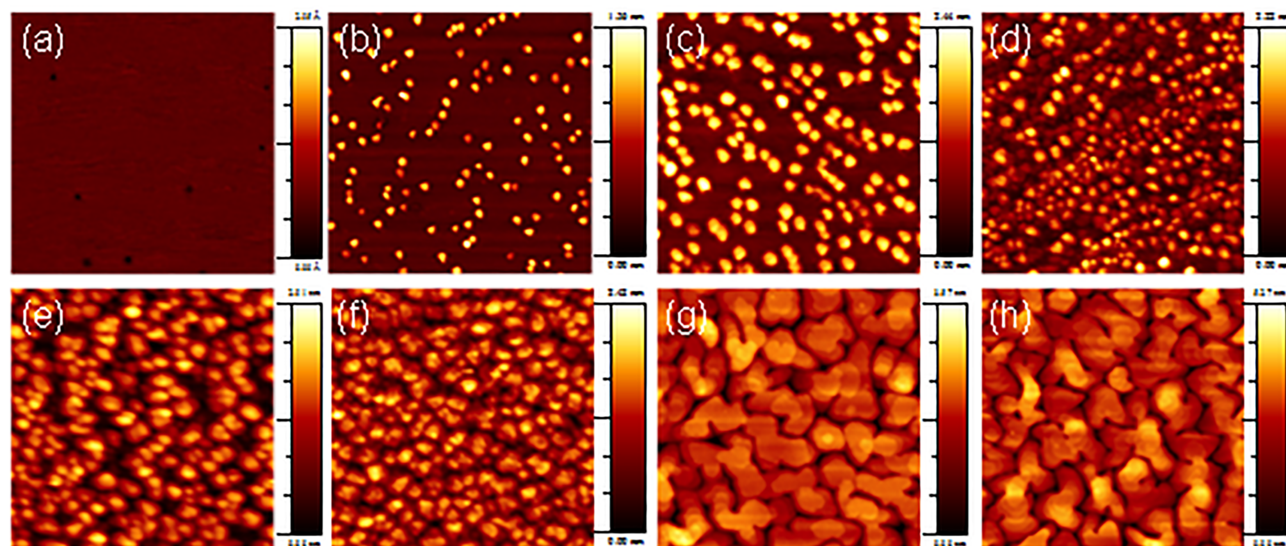

Figure 6. STM images of (a) initial MoS_2 and (b) after 6 s, (c) 12 s, (d) 72 s, (e) 3 min, (f) 10 min, (g) 1 h, and (h) 3 h of Pd deposition. The applied voltage and tunneling current are 1.0 V and 0.5 nA, respectively, for the initial surface and 1.5 V and 0.5 nA for all the Pd-deposited surfaces. All STM images show a 100 nm × 100 nm area.

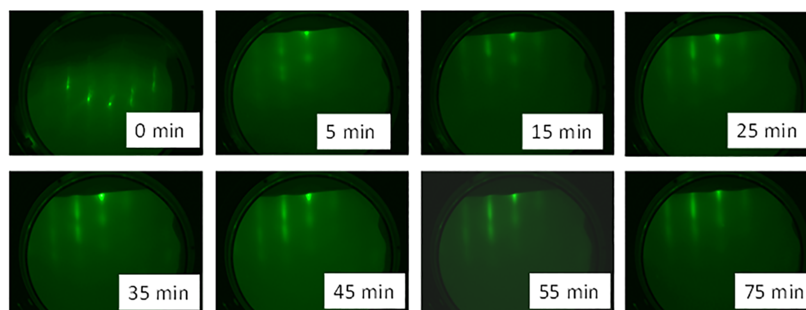

Figure 7. RHEED patterns after 0, 5, 15, 25, 35, 45, 55, 65, and 75 min (4.6 nm) of Pd deposition. The thickness of the Pd film is 4.6 nm is based on the attenuation of Mo 3d signal.

Figure 6 shows the STM images of the MoS_2 initial surface after 6 s, 12 s, 72 s, 3 min, 10 min, 1 h, and 3 h of Pd e-beam evaporation performed in UHV II. The evolution of the Pd film growth mode is consistent with the previous studies of film growth on MoS_2 for catalyst applications.[39] It takes about 3 min of Pd exposure to cover the surface, and the XPS peak position (shown in Figure 4) is seen to gradually change during the deposition.

The islanding of Pd is observed on the MoS_2 surface, and the majority of the islands have a height of 0.8−0.9 nm. The distance between the Pd islands is in the range of a few nanometers. A concomitant peak shift of the Mo 3d spectra, without extra states caused by band bending effects during the successive Pd deposition, is shown in Figure 4. Considering the island growth process during the initial deposition shown in Figure 6b−d, the lateral depletion region is in the range of at least a few nanometers. This indicates a careful doping of the channel is necessary for future field effect transistor devices to avoid the depletion of the contact Pd metal to the channel. The growth mode indicates a strong perturbation of Pd and MoS_2, as the density of metal islands increases randomly on the surface, and is not more favorable to occur at the step edges or the defect sites. It is noted that this growth likely also depends on the substrate of MoS_2 surface layer; this growth mode might vary for a single layer of MoS_2 on SiO_2[14] or on graphene, etc.

The thick deposition after 1 and 3 h (Figure 6g,h) shows the step-terrace structure of the Pd film, suggesting an epitaxial deposition of Pd on the surface. Further indication for the ordered surface structure is provided by RHEED measurement as shown in Figure 7. The diffraction "streaks" suggests that the Pd metal as grown is ordered, and the streaks before and after the gradual Pd deposition suggest that the Pd surface follows the same close-packed structure of the MoS_2 substrate, which is the ⟨111⟩ orientation in palladium. The 0 min image shows the diffraction pattern from the MoS_2 surface, and the image after 75 min (4.6 nm) of Pd deposition shows the diffraction of Pd (111) surface, which is supported by the LEIS result in Figure 8. The orientation is also consistent with reports of the surface characterized by TEM.[39] This epitaxial growth also suggests that the interaction of the Pd and MoS_2 is not weak.

It has been reported that a 1% strain to Pd metal during the initial growth is introduced.[39] But the modification of work function due to possible strain effect is minimal[49] and is discussed further below.

Low-energy ion scattering spectroscopy (LEIS) is an extremely surface sensitive technique, which only detects the outermost layer of the surface atomic composition.[50] Figure 8 shows the LEIS spectra after 75 min (4.6 nm) of Pd deposition from UHV I. The Mo and S are below the LEIS detection limit after the 75 min (4.6 nm) of Pd deposition, which indicates that

DOI: 10.1021/acsami.7b10974
ACS Appl. Mater. Interfaces 2017, 9, 38977−38983

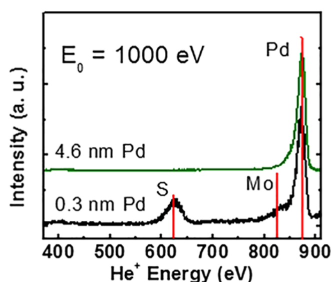

Figure 8. LEIS results of Pd before and after 75 min (4.6 nm) of Pd deposition. He^+ was used as the ion source, and a kinetic energy of 1000 eV was applied.

the diffraction streaks from the RHEED signal originates only from the Pd surface.

The perturbation of the MoS_2 surface by the deposited Pd is also illustrated in the XPS core level spectra of Mo 3d and S 2p as shown in Figure 9. The core level spectra were shifted to the same binding energy so as to compare the line shape with the spectra from the initial surface. From the broadening of the core level spectra upon the Pd deposition during the deposition time of 12 s and 10 min, a perturbation to the MoS_2 surface is expected and is hypothesized to be correlated to the redistribution of charge at the MoS_2/Pd interface. A graphene or boron nitride (BN) layer between Pd and MoS_2 is reported to minimize the perturbation and enable tuning the SBH.[17,51−53]

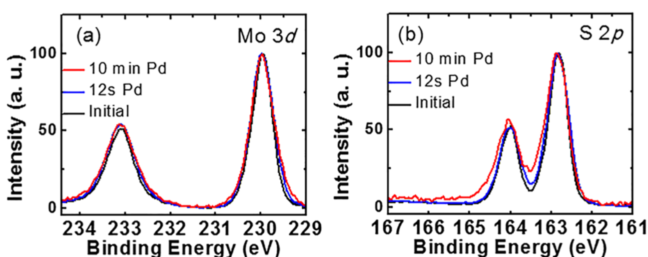

Figure 9. Normalized (a) Mo 3d and (b) S 2p spectra for the initial, after 12 s, and after 10 min of Pd deposition on the MoS_2 bulk surface.

CONCLUSIONS

In summary, a strong band bending effect is observed after Pd was deposited on the MoS_2 bulk surface, which originally exhibits both n- and p-type behavior. The metal work function is found to be located in the middle of the MoS_2 band gap. Successive Pd deposition results in an epitaxial growth mode and is consistent with literature reports. The work function of Pd decrease for the Pd/MoS_2 interface is consistent with the reported theoretical simulations on single-layer MoS_2. Because the work function of Pd is aligned with the middle of the band gap, the SBH is high for both n- and p-type contact purposes, which is also consistent with the high contact resistance from electrical measurements in the literature. To decouple this band bending effect, an interfacial layer to separate the metal and MoS_2 is a possible solution, for example MoO_x, graphene, BN, etc., as already shown in the literature,[6,22,54] resulting in a lower contact resistance.

ASSOCIATED CONTENT

Supporting Information

The Supporting Information is available free of charge on the ACS Publications website at DOI: 10.1021/acsami.7b10974.

Comparison of Mo spectra with UHV systems employed; Mo 3d core level spectra after 10 min of Pd deposition in UHV system 1 (UHV 1) and after 75 min of Pd deposition in the UHV system 2 (UHV 2); a much weaker signal is detected from the UHV system 2; the same final binding energy of the spectra is obtained (PDF)

AUTHOR INFORMATION

Corresponding Author

*E-mail: rmwallace@utdallas.edu (R.M.W.).

ORCID

Rafik Addou: 0000-0002-5454-0315
Stephen McDonnell: 0000-0001-9173-2060
Christopher L. Hinkle: 0000-0002-5485-6600
Robert M. Wallace: 0000-0001-5566-4806

Present Address

S.M.: Department of Materials Science and Engineering, the University of Virginia, Charlottesville, VA 22904.

Notes

The authors declare no competing financial interest.

ACKNOWLEDGMENTS

We thank Ms. Jieyu Liu and Dr. Changhong Wang for their useful discussions. This work is supported in part by the Center for Low Energy Systems Technology (LEAST), one of six centers supported by the STARnet phase of the Focus Center Research Program (FCRP), a Semiconductor Research Corporation program sponsored by MARCO and DARPA, the US/Ireland R&D Partnership (UNITE) under the NSF award ECCS-1407765, and National Natural Science Foundation of China (61504070), the Fundamental Research Funds for the Central Universities, and the Tianjin Natural Science Foundation (15JCYBJC52000).

REFERENCES

(1) Radisavljevic, B.; Kis, A. Mobility Engineering and a Metal-Insulator Transition in Monolayer MoS_2. *Nat. Mater.* **2013**, *12* (9), 815−820.

(2) Laskar, M. R.; Ma, L.; Kannappan, S.; Park, P. S.; Krishnamoorthy, S.; Nath, D. N.; Lu, W.; Wu, Y.; Rajan, S. Large Area Single Crystal (0001) Oriented MoS_2. *Appl. Phys. Lett.* **2013**, *102*, 252108.

(3) Radisavljevic, B.; Radenovic, A.; Brivio, J.; Giacometti, V.; Kis, A. Single-Layer MoS_2 Transistors. *Nat. Nanotechnol.* **2011**, *6* (3), 147−150.

(4) Radisavljevic, B.; Whitwick, M. B.; Kis, A. Integrated Circuits and Logic Operations Based on Single-Layer MoS_2. *ACS Nano* **2011**, *5* (12), 9934−9938.

(5) Chhowalla, M.; Shin, H. S.; Eda, G.; Li, L.-J.; Loh, K. P.; Zhang, H. The Chemistry of Two-Dimensional Layered Transition Metal Dichalcogenide Nanosheets. *Nat. Chem.* **2013**, *5* (4), 263−275.

(6) Chuang, S.; Battaglia, C.; Azcatl, A.; Mcdonnell, S.; Kang, J. S.; Yin, X.; Tosun, M.; Kapadia, R.; Fang, H.; Wallace, R. M.; Javey, A. MoS_2 P-Type Transistors and Diodes Enabled by High Work Function MoOx Contacts. *Nano Lett.* **2014**, *14* (3), 1337−1342.

(7) Yang, L.; Majumdar, K.; Liu, H.; Du, Y.; Wu, H.; Hatzistergos, M.; Hung, P. Y.; Tieckelmann, R.; Tsai, W.; Hobbs, C.; Ye, P. D.

Chloride Molecular Doping Technique on 2D Materials: WS_2 and MoS_2. *Nano Lett.* **2014**, *14* (11), 6275−6280.
(8) Zhang, C.; Johnson, A.; Hsu, C.; Li, L.; Shih, C.-K. Direct Imaging of Band Profile in Single Layer MoS_2 on Graphite: Quasiparticle Energy Gap, Metallic Edge States, and Edge Band Bending. *Nano Lett.* **2014**, *14*, 2443−2447.
(9) Yoon, Y.; Ganapathi, K.; Salahuddin, S. How Good Can Monolayer MoS_2 Transistors Be? *Nano Lett.* **2011**, *11*, 3768−3773.
(10) Kang, J.; Liu, W.; Sarkar, D.; Jena, D.; Banerjee, K. Computational Study of Metal Contacts to Monolayer Transition-Metal Dichalcogenide Semiconductors. *Phys. Rev. X* **2014**, *4* (3), 31005.
(11) Liu, H.; Neal, A. T.; Ye, P. D. Channel Length Scaling of MoS_2 MOSFETs. *ACS Nano* **2012**, *6* (10), 8563−8569.
(12) Azcatl, A.; Qin, X.; Prakash, A.; Zhang, C.; Cheng, L.; Wang, Q.; Lu, N.; Kim, M.; Kim, J.; Cho, K.; Addou, R.; Hinkle, C. L.; Appenzeller, J.; Wallace, R. M. Covalent Nitrogen Doping of MoS_2 by Remote N_2 Plasma Surface Treatment. *Nano Lett.* **2016**, *16* (9), 5437−5443.
(13) Walia, S.; Balendhran, S.; Wang, Y.; Ab Kadir, R.; Sabirin Zoolfakar, A.; Atkin, P.; Zhen, O. J.; Sriram, S.; Kalantar-Zadeh, K.; Bhaskaran, M. Characterization of Metal Contacts for Two-Dimensional MoS_2 Nanoflakes. *Appl. Phys. Lett.* **2013**, *103*, 232105.
(14) Gong, C.; Huang, C.; Miller, J.; Cheng, L.; Hao, Y.; Cobden, D.; Kim, J.; Ruoff, R.; Wallace, R. M.; Cho, K.; Xu, X.; Chabal, Y. J. Metal Contacts on Physical Vapor Deposited Monolayer MoS_2. *ACS Nano* **2013**, *7* (12), 11350−11357.
(15) Tung, R. Recent Advances in Schottky Barrier Concepts. *Mater. Sci. Eng., R* **2001**, *35*, 1−138.
(16) Tung, R. T. Formation of an Electric Dipole at Metal-Semiconductor Interfaces. *Phys. Rev. B: Condens. Matter Mater. Phys.* **2001**, *64* (20), 205310.
(17) Gong, C.; Colombo, L.; Wallace, R. M.; Cho, K. The Unusual Mechanism of Partial Fermi Level Pinning at Metal − MoS_2 Interfaces. *Nano Lett.* **2014**, *14*, 1714−1720.
(18) Guo, Y.; Robertson, J. Schottky Barrier Heights and Band Alignments in Transition Metal Dichalcogenides. *Microelectron. Eng.* **2015**, *147*, 184−187.
(19) Guo, Y.; Liu, D.; Robertson, J. 3D Behavior of Schottky Barriers of 2D Transition-Metal Dichalcogenides. *ACS Appl. Mater. Interfaces* **2015**, *7* (46), 25709−25715.
(20) Kaushik, N.; Nipane, A.; Basheer, F.; Dubey, S.; Grover, S.; Deshmukh, M. M.; Lodha, S. Schottky Barrier Heights for Au and Pd Contacts to MoS_2. *Appl. Phys. Lett.* **2014**, *105* (11), 113505.
(21) Fang, H.; Tosun, M.; Seol, G.; Chang, T. C.; Takei, K.; Guo, J.; Javey, A. Degenerate N - Doping of Few-Layer Transition Metal Dichalcogenides by Potassium. *Nano Lett.* **2013**, *13*, 1991−1995.
(22) Kwak, J. Y.; Hwang, J.; Calderon, B.; Alsalman, H.; Munoz, N.; Schutter, B.; Spencer, M. G. Electrical Characteristics of Multilayer MoS_2 FET's with MoS_2/Graphene Heterojunction Contacts. *Nano Lett.* **2014**, *14* (8), 4511−4516.
(23) Liu, H.; Si, M.; Deng, Y.; Neal, A. T.; Du, Y.; Najmaei, S.; Ajayan, P. M.; Lou, J.; Ye, P. D. Switching Mechanism in Single-Layer Molybdenum Disulfide Transistors: An Insight into Current Flow across Schottky Barriers. *ACS Nano* **2014**, *8* (1), 1031−1038.
(24) Du, Y.; Yang, L.; Liu, H.; Ye, P. D. Contact Research Strategy for Emerging Molybdenum Disulfide and Other Two- Dimensional Field-Effect Transistors Contact Research Strategy for Emerging Molybdenum Disulfide and Other Two-Dimensional Field-Effect Transistors. *APL Mater.* **2014**, *2*, 092510.
(25) McDonnell, S.; Addou, R.; Buie, C.; Wallace, R. M.; Hinkle, C. L. Defect-Dominated Doping and Contact Resistance in MoS_2. *ACS Nano* **2014**, *8* (3), 2880−2888.
(26) McDonnell, S.; Azcatl, A.; Addou, R.; Gong, C.; Battaglia, C.; Chuang, S.; Cho, K.; Javey, A.; Wallace, R. M. Hole Contacts on Transition Metal Dichalcogenides: Interface Chemistry and Band Alignments. *ACS Nano* **2014**, *8* (6), 6265−6272.
(27) Addou, R.; McDonnell, S.; Barrera, D.; Guo, Z.; Azcatl, A.; Wang, J.; Zhu, H.; Hinkle, C. L.; Quevedo-Lopez, M.; Alshareef, H. N.; Colombo, L.; Hsu, J. W. P.; Wallace, R. M. Impurities and Electronic Property Variations of Natural MoS_2 Crystal Surfaces. *ACS Nano* **2015**, *9* (9), 9124−9133.
(28) Spicer, W. E.; Lindau, I.; Skeath, P.; Su, C. Y.; Chye, P. Unified Mechanism for Schottky-Barrier Formation and III-V Oxide Interface States. *Phys. Rev. Lett.* **1980**, *44* (6), 420−423.
(29) Diederich, L.; Küttel, O. M.; Aebi, P.; Schlapbach, L. Electron Affinity and Work Function of Differently Oriented and Doped Diamond Surfaces Determined by Photoelectron Spectroscopy. *Surf. Sci.* **1998**, *418*, 219−239.
(30) Fujimura, N.; Ohta, A.; Makihara, K.; Miyazaki, S. Evaluation of Valence Band Top and Electron Affinity of SiO_2 and Si-Based Semiconductors Using X-Ray Photoelectron Spectroscopy. *Jpn. J. Appl. Phys.* **2016**, *55* (8S2), 08PC06.
(31) Lesker, K. J. http://www.lesker.com/.
(32) Wallace, R. M. In-Situ Studies of Interfacial Bonding of High-k Dielectrics for CMOS Beyond 22nm. *ECS Trans.* **2008**, *16* (5), 255−271.
(33) SPI Supplies; http://www.2spi.com.
(34) Wallace, R. M. In Situ Studies on 2D Materials. *ECS Trans.* **2014**, *64* (9), 109−116.
(35) Addou, R.; Colombo, L.; Wallace, R. M. Surface Defects on Natural MoS_2. *ACS Appl. Mater. Interfaces* **2015**, *7*, 11921−11929.
(36) Nano Science Instruments is a vendor for MoS_2; http://www.nanoscience.com/2.
(37) Herrera-Gomez, A. The software employed for the simultaneous and sequential fitting is AANALYZER; http://www.Aanalyzer.com, http://qro.cinvestav.Mx/~aanalyzer.
(38) ASTM Standard E2108-05, *Standard Practice for Calibration of the Electron Binding-Energy Scale of an X-Ray Photoelectron Spectrometer*, ASTM International: West Conshohocken, PA, www.astm.org.
(39) Perrot, E.; Humbert, A.; Piednoir, A.; Chapon, C.; Henry, C. R. STM and TEM Studies of a Model Catalyst: Pd/MoS_2 (0001). *Surf. Sci.* **2000**, *445*, 407−419.
(40) Hulse, J.; Kuppers, J.; Wandelt, K.; Ertl, G. UV-Photoelectron Spectroscopy from Xenon Adsorbed on Heterogeneous Metal Surfaces. *Appl. Surf. Sci.* **1980**, *6*, 453−463.
(41) Demuth, J. E. Chemisorption of C_2H_2 on Pd (111) and Pt (111): Formation of Thermally Activated Olefinic Surface Complex. *Chem. Phys. Lett.* **1977**, *45* (1), 12−17.
(42) Kubiak, G. D. Two - Photon Photoelectron Spectroscopy of Pd (111). *J. Vac. Sci. Technol., A* **1987**, *5*, 731−734.
(43) Nieuwenhuys, B. E.; Bouwman, R.; Sachtler, W. M. H. The Changes in Work Function of Group Ib and VIII Metals on Xenon Adsorption, Determined by Field Electron and Photoelectron Emission. *Thin Solid Films* **1974**, *21*, 51−58.
(44) Michaelson, H. B. The Work Function of the Elements and its Periodicity. *J. Appl. Phys.* **1977**, *48*, 4729.
(45) Schlaf, R.; Lang, O.; Pettenkofer, C.; Jaegermann, W. Band Lineup of Layered Semiconductor Heterointerfaces Prepared by van Der Waals Epitaxy: Charge Transfer Correction Term for the Electron Affinity Rule. *J. Appl. Phys.* **1999**, *85* (5), 2732−2753.
(46) McDonnell, S.; Brennan, B.; Azcatl, A.; Lu, N.; Dong, H.; Buie, C.; Kim, J.; Hinkle, C. L.; Kim, M. J.; Wallace, R. M. HfO_2 on MoS_2 by Atomic Layer Deposition: Adsorption Mechanisms and Thickness Scalability. *ACS Nano* **2013**, *7* (11), 10354−10361.
(47) Kam, K. K.; Parkinson, B. A. Detailed Photocurrent Spectroscopy of the Semiconducting Group VI Transition Metal Dlchalcogenides. *J. Phys. Chem.* **1982**, *86*, 463−467.
(48) Leigh, G. J. *Gmelin Handbook of Inorganic and Organometallic Chemistry*, 8th ed.; Springer-Verlag: Berlin, 1995.
(49) Abdellatif, M. H.; Ghosh, S.; Liakos, I.; Scarpellini, A.; Marras, S.; Diaspro, A.; Salerno, M. Effect of Nanoscale Size and Medium on Metal Work Function in Oleylamine-Capped Gold Nanocrystals. *J. Phys. Chem. Solids* **2016**, *89*, 7−14.
(50) Brongersma, H. H.; Draxler, M.; de Ridder, M.; Bauer, P. Surface Composition Analysis by Low-Energy Ion Scattering. *Surf. Sci. Rep.* **2007**, *62*, 63−109.

DOI: 10.1021/acsami.7b10974
ACS Appl. Mater. Interfaces 2017, 9, 38977−38983

(51) Farmanbar, M.; Brocks, G. Controlling the Schottky Barrier at MoS_2/metal Contacts by Inserting a BN Monolayer. *Phys. Rev. B: Condens. Matter Mater. Phys.* **2015**, *91* (16), 161304.
(52) Su, J.; Feng, L.; Zeng, W.; Liu, Z. Controlling the Electronic and Geometric Structures of 2D Insertions to Realize High Performance metal/insertion−MoS_2 Sandwich Interfaces. *Nanoscale* **2017**, *9* (22), 7429−7441.
(53) Su, J.; Feng, L. P.; Zhang, Y.; Liu, Z. The Modulation of Schottky Barriers of Metal-MoS_2 Contacts via BN-MoS_2 Heterostructures. *Phys. Chem. Chem. Phys.* **2016**, *18* (25), 16882−16889.
(54) Du, Y.; Yang, L.; Zhang, J.; Liu, H.; Majumdar, K.; Kirsch, P. D.; Ye, P. D. MoS_2 Field-Effect Transistors with Graphene/Metal Heterocontacts. *IEEE Electron Device Lett.* **2014**, *35* (5), 599−601.

DOI: 10.1021/acsami.7b10974
ACS Appl. Mater. Interfaces 2017, 9, 38977−38983